ANDRIÉ

JOURNAL OF GEOPHYSICAL RESEARCH, VOL. 94, NO. C1, PAGES 855-870, JANUARY 15, 1989

KINEMATICS OF CO_2 FLUXES IN THE TROPICAL ATLANTIC OCEAN DURING THE 1983 NORTHERN SUMMER

Véronique C. Garçon,[1] Laurent Martinon,[1] Chantal Andrié,[2] Patrick Andrich,[3] and Jean-François Minster[1]

Abstract. CO_2 evasion within the Atlantic equatorial belt (5°N-5°S) increases from the east to the west [Andrié et al., 1986]. Many factors contribute the variations of pCO_2 in the equatorial surface waters. To assess their relative importance, a kinematic box model is developed. A 2° x 2° box whose depth is defined by the 24.90°/$_{oo}$ isopycnal level flows westward from 4°W to 38°W within the Equator-2°S band with the south equatorial current. Time (zonal) evolution of nitrate, total CO_2, total alkalinity and mass, and of the corresponding water pCO_2, are simulated taking into account advection, meridional divergence, diffusion, biological activity, and gas exchange. Initial and boundary conditions are taken from the FOCAL 4 (July-August 1983) data set. The flow field is based on climatology. The ability of the model to reproduce the observed FOCAL data, as well as the correct orders of magnitude of the adjustable parameters K_v (vertical mixing coefficient) and J_{max} (maximum nitrate uptake rate), as compared with independent estimates, suggests that all major terms controling the equatorial Atlantic CO_2 values are considered. Advection fluxes dominate the CO_2 balance. The sinks due to biological consumption approximately balance the inflow from the core of the Equatorial Undercurrent by diapycnal mixing. Calculated new production J_c values vary from east to west between 17 and 1 mol C/m^2/yr, given K_v = 5 x 10^{-4} m^2/s. Isopycnal mixing is negligible. Degassing plays a minor role in the total CO_2 budget. Estimating the biological uptake of nutrients should be a very useful constraint for estimating equatorial divergence.

1. Introduction

The world ocean is believed to act as a sink for atmospheric CO_2, taking up about half the excess CO_2. However, the ocean response does vary seasonally and geographically. Globally, the high-latitude regions behave as a strong CO_2 sink. The subtropical gyre areas are mostly low intensity CO_2 sinks or sources, whereas the low-latitude zones are considered a strong CO_2 source.

In this paper we focus our attention on the outgassing equatorial belt in the tropical Atlantic Ocean, where CO_2 evasion markedly increases from the east to the west [Smethie et al., 1985; Andrié et al., 1986].

The work we present here is a simple approach, elaborating on the working scenario suggested by Smethie et al. [1985]: The increase of CO_2 partial pressure from east to west is explained by warming of sea surface waters which upwell in the eastern area and flow westward along the South Equatorial Current. Andrié et al. [1986] further argue that the gas transfer coefficient significantly increases to the west due to increase in wind velocity. Here we develop a kinematic "Lagrangian" box model that we treat as a forward problem. The box will flow westward within the equatorial band. The zonal evolution of the chemical tracer concentrations (nitrate NO_3^-), total dissolved inorganic carbon (Σ CO_2), total alkalinity (Alk) and of the surface water pCO_2 are simulated, taking into account advection, meridional divergence, diffusion, biological activity, and gas exchange. We use data from the FOCAL 4 cruise in the 1983 boreal summer (July 1 to August 6) (FOCAL: Programme Français Océan Climat en Atlantique Equatorial). This particular season was selected because it constitutes the most extensive data set among the five geochemical FOCAL cruises, and a "normal" hydrological situation of the equatorial Atlantic Ocean. The model allows us to assess the relative importance of the various factors contributing to variation of pCO_2 in surface waters. We are also able to investigate the sensitivity of the model to changes in the vertical diffusion coefficient and in the flow field representation.

The paper is organized as follows. Section 2 describes the basics of the model, and section 3 presents the FOCAL 4 data set. The simulation results are given in section 4, and a discussion of the implications of our findings follows in section 5.

2. The Model

2.1. Geographical Limits

A few factors guided the choice of the geographical limits. The model extends from the Equator to 2°S, and in the east-west direction from 4°W to 38°W, with a 2° resolution in longitude (Figure 1). In the vertical, the bottom of the box is defined by the σ_θ = 24.90°/$_{oo}$ isopycnal surface.

Throughout the year, the swifter part of the South Equatorial Current (SEC) flows westward

[1] UM39, Centre National d'Etudes Spatiales/GRGS: Groupe de Recherche de Géodésie spatiale, Toulouse, France.

[2] Laboratoire de Géochimie Isotopique-LODYC: Laboratoire d'Océanographie Dynamique et de Climatologie, Département de Physico-Chimie, Gif-sur-Yvette, France.

[3] Laboratoire d'Océanographie Dynamique et de Climatologie, Université Pierre et Marie Curie, Paris, France.

Paper number 88JC03026.
0148-0227/89/88JC-03026$05.00

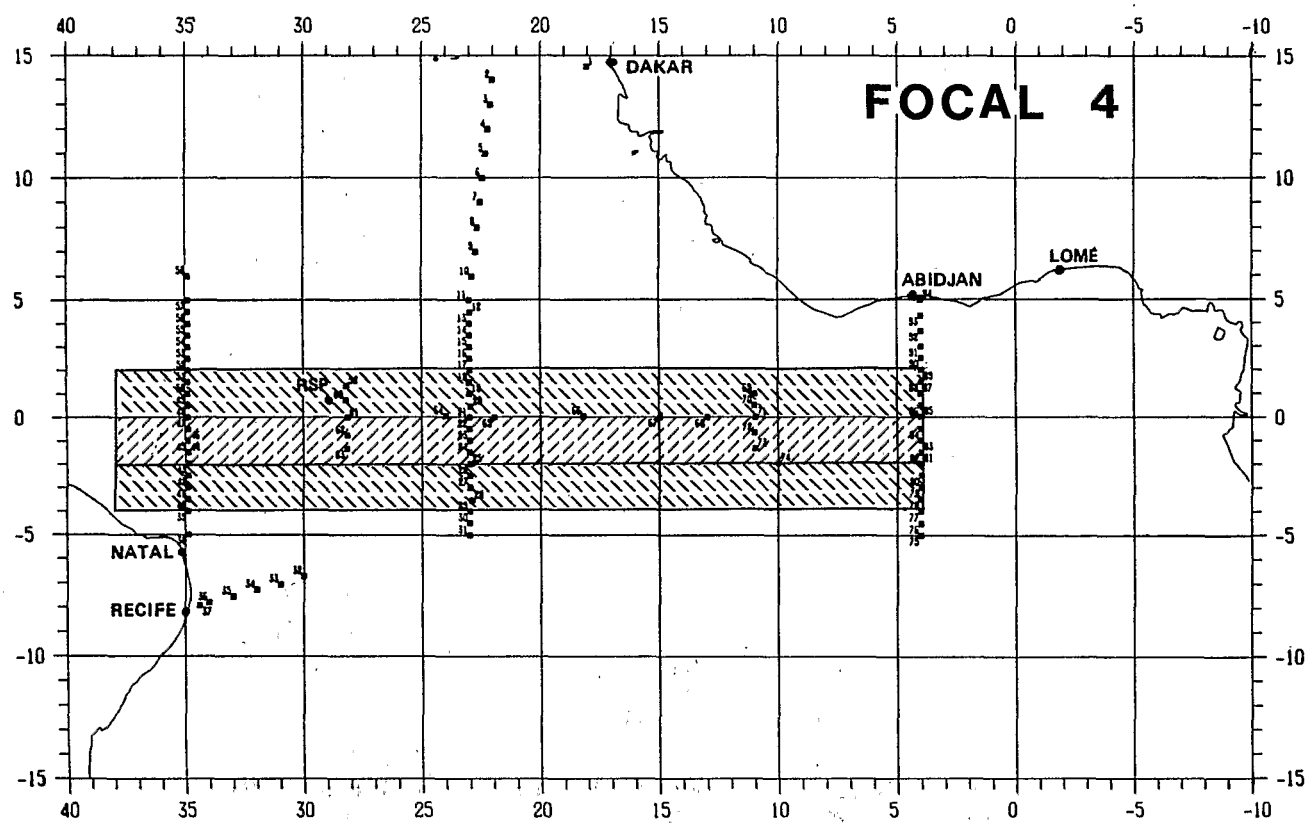

Fig. 1. Map of the FOCAL 4 cruise stations (July 1 to August 6, 1983). Middle shaded section indicates the geographical extension of the model, and top and bottom shaded sections indicate the northern and southern bands defined as the model boundaries.

across the Atlantic Ocean in a relatively large band between 4°N-6°N and 8°S. From July to December the intensification of the southeast trade winds linked to the northward migration of the Intertropical Convergence Zone (ITCZ) causes an acceleration of the westward SEC. It then weakens from January to June as the relaxation of the trade winds proceeds [Richardson and McKee, 1984; Arnault, 1984]. In the equatorial upwelling of the Gulf of Guinea at 4°W, Voituriez et al. [1982] identify in the 1978 cold season (August) a meridional divergence zone between 2°S and 2°30S which separates two distinct branches of the SEC. This zone coincides with significant cooling and nutrient enrichment of the surface waters. Voituriez [1983] localizes the equatorial divergence at 4°W between 0°30S and 1°30S in July 1975 and 1977, and around 2°S in June 1979. For July 1983, Figure 2 shows that nitrate-enriched surface waters appear near 1°S-2°S, 0°30S-2°S, and 0°-1°S along the 4°W, 11°W, and 23°W meridian sections, respectively. Similarly, the temperature surface minimum and the pCO_2 surface maximum are found within these latitudinal bands [Andrié et al., 1986; Oudot et al., 1988]. Let us recall that we want to capture the essential characteristics of surface waters which upwell during the cold season in the Gulf of Guinea in order to follow them as they flow zonally with the SEC. We therefore choose to center our 2° x 2° box on the Equator-2°S band, where the equatorial divergence is well pronounced.

The 4°W-38°W extension of the model in longitude is dictated by the location of the five meridional transects along 4°W, 11°W, 23°W, 28°W, and 35°W of the FOCAL 4 campaign (Figure 1).

The 2° step in longitude represents the approximate distance over which all the processes governing the total CO_2 evolution are resolved. Roughly, during FOCAL 4 in the Equator-2°S band, surface mixed layers of 20-40 m and 80 m coincide with CO_2 transfer coefficients of 4 and 10 cm/h, respectively, corresponding to wind speeds ranging between 4.5 and 7 m/s [Andrié et al., 1986]; so we can deduce a characteristic gas exchange time of the order of 8 to 40 days. One can reasonably say that, in the equatorial upwelling of the eastern Atlantic, CO_2 removal from the euphotic zone by new production occurs on a several-day time scale, whereas the mixing processes have slower kinetics of about 1 month. The typical velocity of the westward SEC is about 30-40 cm/s, as indicated by current profiler measurements [Hisard and Hénin, 1984], by drifting buoy data [Reverdin and McPhaden, 1986] for July-August 1983, and by historical ship drift data for the boreal summer season [Richardson and McKee, 1984]. During 8 days, the displacement of the surface water is thus approximately 2° in longitude.

The hydrological data along each of the five meridian sections between 2°N and 4°S [Hénin et al., 1986] allow us to identify a mixing scheme between three water types: Low salinity, warm surface water, high-salinity core water of the Equatorial Undercurrent (EUC), and subthermocline

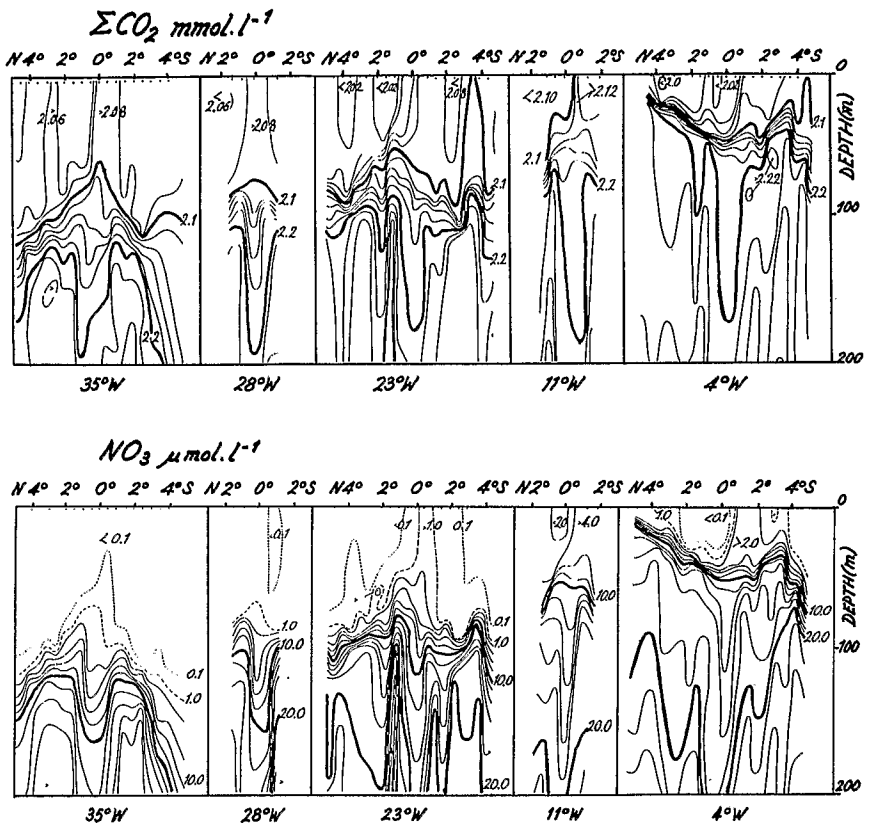

Fig. 2. Sections of total CO_2 (ΣCO_2) (mmol/L), and nitrate (NO_3^-) (µmol/L) concentrations to 200 m along the 4°W, 11°W, 23°W, 28°W, and 35°W meridians during the FOCAL 4 cruise (July 1983). The contour intervals are 0.02 mmol/L and 2 µmol/L for ΣCO_2 and NO_3^-, respectively, or are indicated in the figure for the surface waters.

water below a TS point of 15.7°C and 35.65°/₀₀. The first two have a composition varying zonally, whereas subthermocline waters are almost invariable. The σ_θ density of 24.90°/₀₀ is selected as the bottom of the box because it includes the surface mixed layer and lies above the depth of the EUC salinity maximum. The box depth varies zonally in the range 30-100 m corresponding to that of the 24.90°/₀₀ isopycnal horizon, and so does the volume of the box (Figure 3).

2.2. Tracer Conservation Equations

The basic building block of our box model is the integral form of the conservation equation of a stable tracer C:

$$V \cdot \frac{\delta C}{\delta t} = \int_{surf} (K \cdot \nabla C - j_w C)\, ds + Q \qquad (1)$$

Equation (1) states that the time rate of change of the mean concentration C in the box of volume V (Figure 4a) is given by the integrated flux of tracer across the interior boundary surface of the box plus the box source/sink function Q. Q includes the amount of tracer exchanged per unit time across external boundaries and produced via all chemical and biological processes inside the box. Simplifying the flux integral over the box boundary surface [see Keeling and Bolin, [1967] for a general discussion], the tracer conservation equation (1) can be written

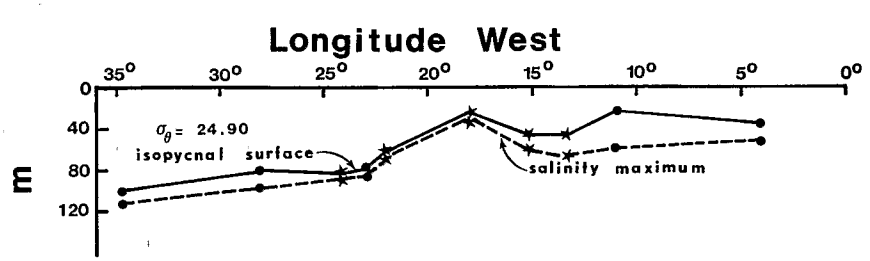

Fig. 3. Average depths of the σ_θ = 24.90°/₀₀ isopycnal surface (solid curve) and of the EUC salinity maximum (dashed curve) between the Equator and 2°S. Stars denote individual stations (64 to 68) along the Equator.

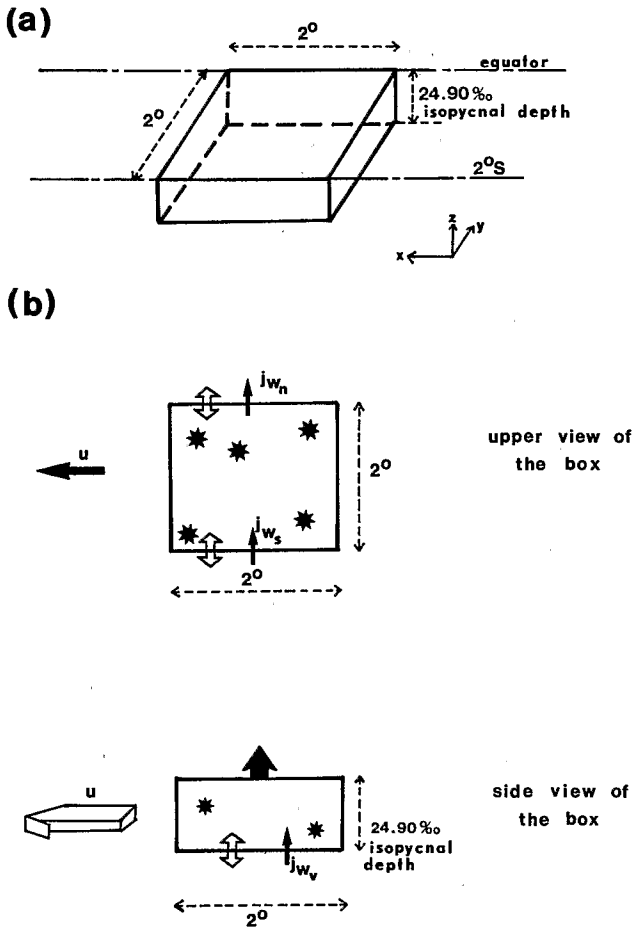

Fig. 4. (a) Schematic diagram of the 2° x 2° box flowing between 0° and 2°S. (b) Upper and side views of the box. Symbols represent the diffusion (open arrow), advection (thin solid arrow), gas exchange (thick solid arrow), and biological activity processes (stars). The u denotes the box average zonal velocity, and j_{W_N}, j_{W_S} and j_{W_V} denote advection across the northern, southern, and bottom boundaries of the box, respectively.

$$V \cdot \frac{\delta C}{\delta t} = \sum_i A_i \left[\frac{(C-C_i) \cdot K_i}{\Delta l} - \frac{(C+C_i)}{2} \cdot \bar{j}_{W_i} \right] + Q \quad (2)$$

where summation is over the northern, southern, and bottom surfaces of the box. Summation over the eastern and western surfaces of the box is omitted, since the box is advected zonally with a mean westward velocity over δt. Here j_W (in m/s) represents the spatial mean advection across a boundary surface, positive when directed outward from the box. The "apparent" isopycnal and diapycnal eddy diffusion coefficients K_i (in m^2/s) parameterize the effect of spatial fluctuations of the tracer concentrations and of the advection field which are not resolved by the spatial resolution of the model. A_i denotes any boundary surface (in m^2), and Δl the distance (in meters) of interest for the concentration gradient.

The chemical tracers for which we choose to follow the zonal evolution of the concentration across the Atlantic basin are the following: nitrate (NO_3^- in μmol/kg), total CO_2 (ΣCO_2 in μmol/kg), and total alkalinity (Alk in μeq/kg). The Q term is thus in μmol or μeq per unit time.

To assure mass conservation for the box, we write a mass balance equation of the form

$$\sum_i J_{W_i} = 0 \quad (3)$$

where the water transports $J_W = A.j_W$ are in 10^6 $m^3/s \approx 1$ Sv, and the summation is over the northern, southern, and bottom interface areas of the box. It of course includes the mass flux due to variation of the box volume V with time. Combining (2) and (3), and discretizing in time with a Euler forward scheme, the tracer conservation equation can be rewritten as

$$(C\ V)_{n+1} = (C\ V)_n + \Delta t \cdot \phi_n$$

$$\phi = \sum_{\substack{i = \\ \text{north} \\ \text{south} \\ \text{bottom}}} \left[\frac{A_i\ K_i\ (C - C_i)}{\Delta l} - \frac{(C + C_i)\ J_{W_i}}{2} \right] + Q \quad (4)$$

The forward problem we treat is thus defined by specifying water fluxes j_{W_i}, mixing coefficients K_i, sources/sinks Q, the tracer concentrations at the boundaries (north of the Equator, south of 2°S latitude, and the EUC) of the box, and the time step Δt, as the ratio of the 2° longitude distance over the average zonal velocity of the box. We also append the appropriate initial conditions (that is, we define the tracer concentrations in the box) at 4°W longitude. Equations (4) are used to solve for the box concentrations of NO_3^-, Alk, and ΣCO_2. The way we proceed is the following (Figure 4b): Over Δt, we consider the advection, eddy diffusion, and biological processes to occur. We then compute the CO_2 partial pressure in surface seawater, the corresponding net CO_2 flux across the air-sea interface, and the resulting box ΣCO_2 concentration by deducing the carbon loss due to the gas exchange. The box flows 2° westward, and we reiterate the procedure.

2.3. Parameterization of Physical Processes

2.3.1. The flow field. We obviously need to know the westward SEC velocities within the Equator -2°S band in the tropical Atlantic Ocean during the boreal summer season. We first use the monthly mean surface velocities for the month of August derived from historical ship drift data [Richardson and Walsh, 1986]. They represent an average over a 2° of latitude by 5° of longitude box of all individual ship drift measurements made during the 1875-1976 period (Figure 5a). We first decompose each of the velocity vectors along the Equator and 2°S into its zonal and meridional components. We then compute the box average zonal velocity along 1°S each 2° of longitude by linear interpolation (Figure 5b). While so doing, we thus set the time step Δt of integration as the time required by the SEC to flow 2° westward at its given zonal velocity. The meridional component of the velocity leaving the box at the northern boundary (along the Equator) is from the Richardson and Walsh climatology

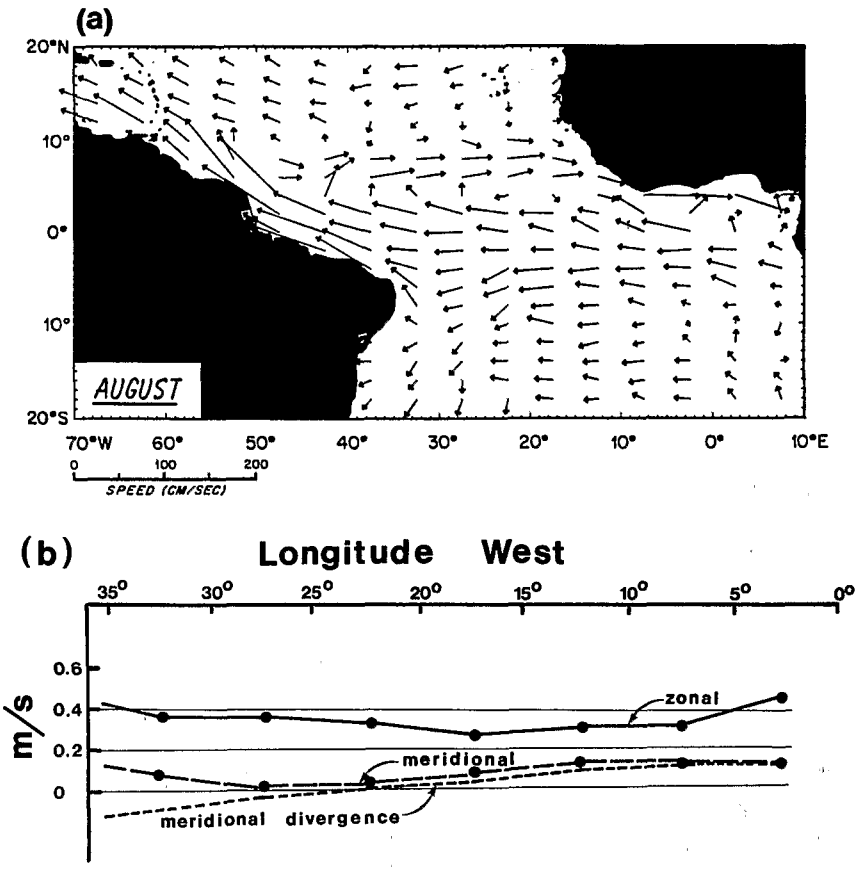

Fig. 5. (a) Map of surface velocity vectors in the tropical Atlantic Ocean for the month of August. Speed is proportional to the length of the tail of a vector [from Richardson and Walsh, 1986]. (b) Box average zonal velocity (along 1°S) (solid line), meridional component of the velocity at the northern boundary of the box (along the Equator) (long-dashed line), and meridional velocity divergence (short-dashed line) (in m/s) across the Atlantic basin from 4°W to 35°W.

(Figure 5b), and we derive the southern component at 2°S latitude, so that mass continuity in the 2° x 2° box is satisfied (equation (3)). Other flow fields will be used for comparison (see sections 4.2. and 4.3.). We make the assumption that the vertical velocity j_{w_V} is equal to zero. This implies that the zonal change of the volume of the box is associated with the meridional velocity divergence (Figure 5b) and that the upwelling flux is only diffusive.

2.3.2. The Mixing Coefficients. As suggested by Pacanowski and Philander [1981], the vertical eddy diffusion K_v depends upon the Richardson number R_i, according to

$$K_v = \frac{K_{v_o}}{(1 + aR_i)^n} + K_b$$

with K_b = 1 cm^2/s, n = 2, a = 5, and K_{v_o} = 100 cm^2/s. K_b is a background vertical eddy viscosity coefficient and K_{v_o}, a, and n are adjustable parameters. The values given above for these adjustable parameters are the ones that gave the most realistic simulations in Philander's model. R_i varies both in latitude and longitude. Here, for simplicity, we use the R_i value as calculated by Provost and Suk [1987] in the surface layers for an averaged vertical structure of the currents at the Equator. Considering then the zonal change of scale of the vertical density gradient, we derive values for the vertical eddy diffusion coefficient K_v ranging from 10^{-4} to 10^{-3} m^2/s.

We assign the lateral (horizontal) eddy diffusion coefficient a value of 5 x 10^2 m^2/s, which is in the range of 10^2 to 2 x 10^3 m^2/s as documented in Gargett's [1984] review.

2.4. Parameterization of Biogeochemical Processes

The Q term in (4) is simply a sink term for the three tracers of interest here. Biological consumption affects nitrate, total alkalinity, and total CO_2 concentrations inside the box, whereas gas exchange across the air-sea interface will alter only total CO_2. We do not consider nutrient inputs from the atmospheric source.

2.4.1. Biological Activity. Phytoplankton growth that we have to define here is driven by "new" nitrogen supplied to the euphotic zone of the ocean via divergence and mixing. This concept of "new" versus recycled nitrogen corresponds to the separation of physical input from biological cycling [Dugdale and Goering, 1967; Eppley and

Peterson, 1979]. We describe the rate of nitrate uptake by Michaelis-Menten kinetics:

$$J_{NO_3^-} = J_{max} \frac{[NO_3^-]}{K_s + [NO_3^-]} \quad (5)$$

where $J_{NO_3^-}$ and J_{max} are the nutrient and maximum nutrient uptake rates, respectively (in μmol per unit time), K_s is the half-saturation constant (defined as the nutrient concentration at which the rate is one-half the maximum, in μmol/kg), and $[NO_3^-]$ the ambient nitrate concentration (in μmol/kg). As a first step, we considered $[NO_3^-]$ as the observed FOCAL nitrate concentrations, but in the results presented herein, $[NO_3^-]$ is a state variable of the model. We attribute the half-saturation constant for nitrate uptake K_s a value of 0.5 μmol/kg, which is in the range of 0.1-0.7 μmol/kg as reported by Eppley et al. [1969] for oceanic phytoplankton species. The model is then adjusted to represent the data through a single coefficient, the maximum nutrient uptake rate J_{max}. We relate the photosynthetic utilization of CO_2 to that of NO_3^- using the Redfield C/N ratio of 103/16 as revised by Takahashi et al. [1985]. We consider the ratio $C_{organic}/C_{CaCO_3}$ to be equal to 4. Calcium carbonate production ($CaCO_3$) uses up two positive charges and correspondingly reduces the alkalinity. In addition, for each 4 mol of carbon incorporated by phytoplankton through photosynthesis, about 0.6 mol of nitrogen are incorporated so raising the alkalinity by 0.6 eq [Broecker and Peng, 1982]. We further consider that decomposition of organic matter and dissolution of carbonates occur in the water column below the 24.90°/$_{oo}$ isopycnal surface.

In summary, we can write the sink term due to biological activity as

$$Q_{NO_3^-} = - J_{NO_3^-}$$

$$Q_{\Sigma CO_2} = - 5\, C_{CaCO_3}/C_{org} \cdot C/N \cdot J_{NO_3^-} \quad (6)$$

$$Q_{Alk} = - 1.4/5 \cdot Q_{\Sigma CO_2}$$

in which $Q_{NO_3^-}$ and $Q_{\Sigma CO_2}$ are in μmol per unit time, and Q_{Alk} in μeq per unit time.

2.4.2. Gas Exchange. The net flux of CO_2 between the ocean and the atmosphere is given by

$$F = 0.24\, k\, S\, \Delta pCO_2 \text{ (in mmol/m}^2 \text{ d)} \quad (7)$$

where k is the CO_2 transfer coefficient (in cm/h [Liss, 1973; Broecker and Peng, 1974]), S is CO_2 solubility in seawater (in mol/l atm [Weiss, 1974]), and ΔpCO_2 is the difference between the seawater pCO_2 and atmospheric pCO_2 (in μatm). For a given gas the transfer coefficient k depends on wind speed and on sea surface temperature. We describe this dependency by the relationship derived by Liss and Merlivat [1986].

We compute the partial pressure of CO_2 in seawater from the total alkalinity and total CO_2 following the equations given by Broecker and Takahashi [1978]. The dissociation constants of carbonic acid and boric acid are taken from Mehrbach et al. [1973], and Lyman [1956], respectively. The total borate concentration is computed using the relation given by Culkin [1965]. The temperature and salinity values inside the boxes are supposed as given: The model was not set to simulate these parameters. We finally calculate the box total CO_2 concentration by subtracting the carbon loss over the time step Δ t due to the net CO_2 flux across the air-sea interface.

3. Data

We use the geochemical data from the FOCAL 4 cruise in the 1983 boreal summer (July 1 to August 6). Three regions of the tropical Atlantic Ocean were regularly sampled in a narrow-mesh net: (1) the 4°W meridian between 5°N and 5°S, (2) from 22°W to 23°W between 14°N and 5°S, and (3) the 35°W meridian between 5°N and 5°S (Figure 1). Two other smaller transects along the 11°W and 28°W meridians were sampled between 2°S and 1°30N. We discard data from the isolated stations along the Equator (stations 64 to 68) because they do not represent average properties over the 2° x 2° box on the Equator-2°S band. For each station we have the following information at 12 depths in the upper 500 m of water. Data include hydrography (temperature, salinity), chemical properties (dissolved oxygen, phosphate, nitrate, nitrite, pH, total CO_2 (ΣCO_2) concentration in water, CO_2 partial pressure in surface water (at 1-m depth), and CO_2 partial pressure in the atmosphere (at 10-m height above the sea surface)), and biological properties (chlorophyll a and phaeophytin a) [Hénin et al., 1986; Oudot et al., 1988].

No measurements of total (titration) alkalinity were performed during all FOCAL cruises. In order to compute the partial pressure of CO_2 in seawater, we need to "reconstruct" total alkalinity values. We will use salinity measurements, as salinity is the first controling factor of alkalinity. However, we will allow a varying relationship between salinity and alkalinity from east to west, to account for the effects of higher production in the Gulf of Guinea than in the west. The way we proceed is illustrated in Figure 6. In this total alkalinity versus salinity plot, we report the Transient Tracers in the Ocean/Tropical Atlantic Study (TTO/TAS) and GEOSECS values of the upper 500 m of water of all stations comprised between 12°S and 11°N in the Atlantic Ocean. The GEOSECS values first have to be corrected from the 14-μeq/kg offset with the TTO values [see Takahashi et al., 1985]. Then a set of two linear relationships (lines 1 and 2, the slope break being at a salinity of 36°/$_{oo}$) is derived between alkalinity and salinity for the western Atlantic Ocean. A third linear relationship is derived for the eastern Atlantic Ocean (GEOSECS East Stations) (Figure 6). In order to describe the zonal evolution of the alkalinity-salinity relationship, we linearly increase the constant A (line 3, Figure 6) from 4°W to 23°W, where salinities equal or greater than 36°/$_{oo}$ appear. Total alkalinity values for the FOCAL 4 cruise are then derived from these relationships and from the FOCAL 4 salinities.

We now establish the tracer concentrations at

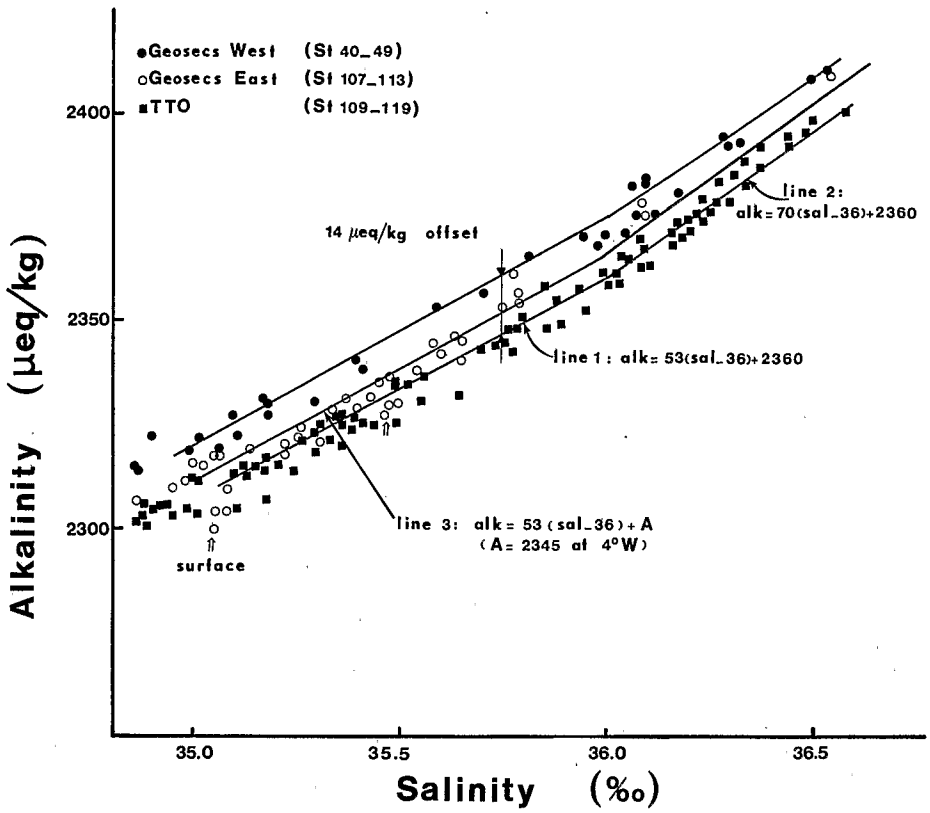

Fig. 6. Alkalinity (total) (μeq/kg) versus salinity (°/₀₀) for GEOSECS and TTO/TAS upper 500 m of water (stations between 12°S and 11°N). Lines 1 and 2, western; line 3, eastern tropical Atlantic Ocean. See text.

the boundaries, and the box average tracer concentrations in the Equator-2°S band along the 4°W, 11°W, 23°W, 28°W, and 35°W meridians. The concentrations, at 4°W longitude, will be the initial box conditions. These box average tracer concentrations will be compared with the box concentrations calculated by the model along the five meridians. The northern and southern boundaries are defined as being the 2°N-Equator and 2°S-4°S bands. For each 2° x 2° box (the northern and southern boundary boxes and the central box) along the five FOCAL transects (Figure 2 and Oudot et al. [1988]), a weighted average of temperature, salinity, nitrate, total CO_2, and alkalinity for the depth interval corresponding to that of the 24.90°/₀₀ isopycnal horizon is calculated. The tracer concentrations at the bottom boundary of the central box are the tracer values corresponding to the salinity maximum in the high-salinity core water of the EUC (Figure 2 and Oudot et al. [1988]). To generate these tracer concentrations along the zonal extension of the model (northern, southern and bottom), we linearly interpolate between the tracers values of the five sampled meridians.

During the FOCAL 4 cruise, the mean CO_2 atmospheric partial pressure along the 4°W, 23°W, and 35°W meridians in the Equator-5°S band varies between 334 and 336 μatm [Andrié et al., 1986]; we therefore assign a constant value of 335 μatm to the atmospheric pCO_2. The surface CO_2 partial pressure data in seawater in the central Equator-2°S band are taken from Andrié et al. [1986]: They will be compared with the pCO_2 computed by the model. Mean wind values of the FOCAL 4 cruise necessary to compute the CO_2 transfer coefficient K (equation (7)) are taken from the atlas of Tourre et al. [1986].

4. Results

The results of the model are first discussed by comparing the calculated and observed concentrations along the Equator-2°S band (Figure 7). Essentially, two parameters, K_v and J_{max}, allow an adjustment of the model.

4.1. Sensitivity to the Vertical Eddy Diffusion Coefficient

Several simulations have been carried out to study the effect of varying the vertical eddy diffusion coefficient K_v. It appears that for a given K_v, there corresponds an optimal maximum nutrient uptake rate J_{max} producing the best fit to the data. Figure 7 shows simulation results for two values of vertical eddy diffusion coefficient, K_v = 5 and 10 x 10^{-4} m^2/s, corresponding to values of J_{max} of 5 and 10 x 10^9 μmol/s, respectively. The general trend of variation of the tracer concentrations has been quite well predicted.

Alkalinity-estimated values increase westward from 2320 to 2374 μeq/kg following the salinity increase (35.54 to 36.20°/₀₀) due to evaporation and mixing with water from the high-salinity core. Alkalinities obtained by the model with K_v

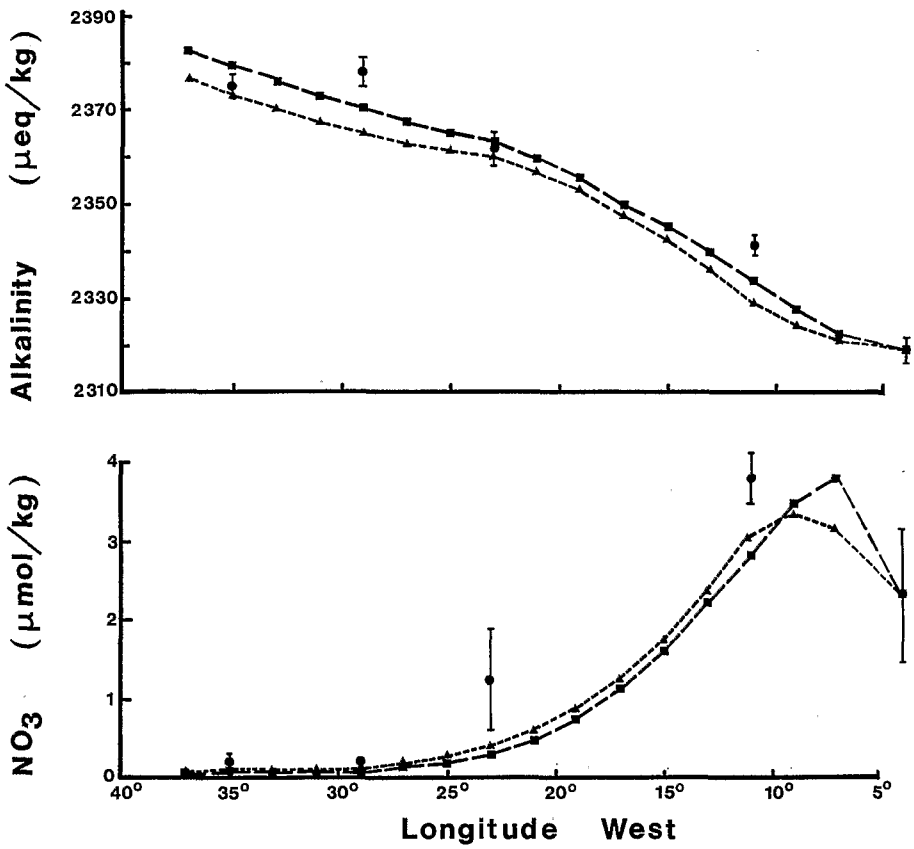

Fig. 7. Alkalinity (total) (μeq/kg), nitrate (NO_3^- (μmol/kg), total CO_2 ΣCO_2 (μmol/kg), partial pressure of CO_2 pCO_2 (μatm), CO_2 flux from the ocean to the atmosphere (mmol/m^2 day) versus longitude within the Equator-2°S band. The simulation results, in cases K_V ▫ 5 and 10 x 10^{-4} m^2/s, are indicated by triangles and squares, respectively, and the 2° x 2° box average tracer concentrations from FOCAL 4 measurements are shown by solid circles (for pCO_2, data are surface measurements). Along the 4°W, 11°W, 23°W, 28°W, and 35°W meridians, the error bars represent data dispersion. A constant mean atmospheric pCO_2 of 335 μatm is assigned. The observed CO_2 flux is obtained by introducing the measured surface water pCO_2 during FOCAL 4 in (7). The flow field is derived from Richardson and Walsh [1986].

= 10^{-3} m^2/s are closer to the "data" than those with K_V = 5 x 10^{-4} m^2/s. However, in both cases, the model underestimates the reconstructed alkalinities (largest difference equal to 13 μeq/kg) until 28°W of longitude, and slightly overestimates them (by 5 μeq/kg) west of 28°W, in the case of large K_V. In view of the way we reconstructed alkalinities, this result is not surprising, possibly due to larger effect of production in the Gulf of Guinea (in July) than estimated using the GEOSECS data (in March and October). In any case, this is of little significance for the other parameters. The observed distributions reveal a strong nitrate enrichment (≈ 3.8 μmol/kg) along the 11°W meridian which coincides with peaks in total CO_2 (≈ 2067 μmol/kg) and surface pCO_2 (≈ 402 ppm). The upwelling diffusive flux feeds the SEC in nitrate and ΣCO_2, thereby producing predicted levels of nitrate (3.8 μmol/kg) and total CO_2 (2061 μmol/kg) which exhibit this enrichment. It occurs, however, slightly shifted in longitude (8°-10°W) as compared with the data. Westward of 10°W, the results for the two K_V values are quite similar for nitrate as well as for total CO_2. However, the rich nitrate waters in the Gulf of Guinea become overdepleted in the model between 10°W and 28°W, the simulated NO_3^- values being closer to the lower bound of the error bar of the observed NO_3^- values. Similarly, along the 11°W meridian, we obtain simulated levels of ΣCO_2 concentrations that are too low (by 13 μmol/kg). In the western Atlantic, the agreement between measured and predicted nitrate and total CO_2 concentrations is achieved whitin error bars.

One can say that the model is able to predict the general pattern of the surface water pCO_2 and of the CO_2 escape to the atmosphere from the east to the west. However, the model slightly overestimates seawater pCO_2 and gas exchange. This is not so surprising as (1) we compare measured surface pCO_2 with simulated box average pCO_2, and consequently (2) we derive degassing from this box average, while the "observed" flux is obtained by introducing the measured surface pCO_2 in (7). Notwithstanding this remark, simulated and measured seawater pCO_2 values differ by no more than 14 μatm in the eastern

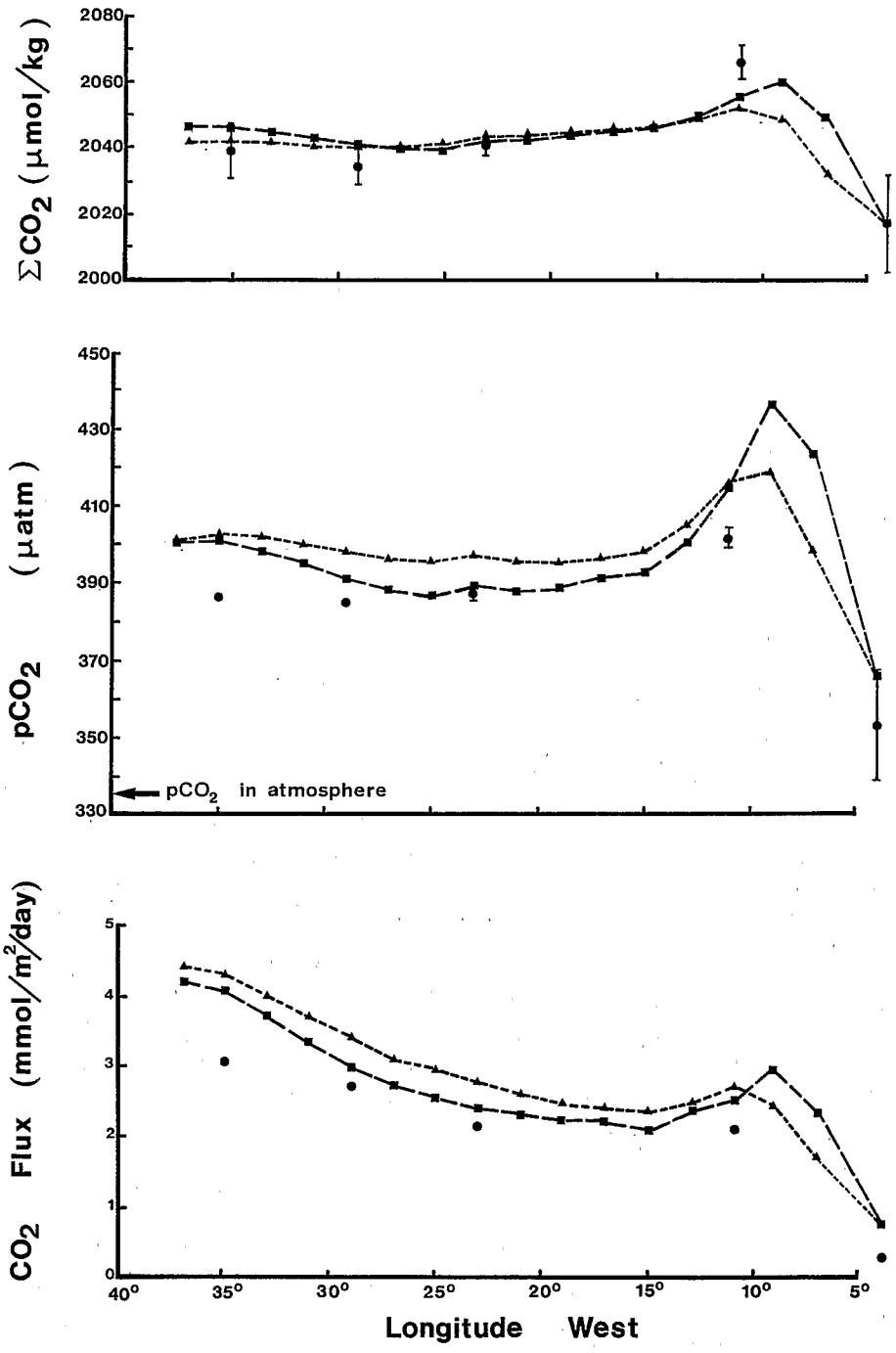

Fig. 7 (continued)

Atlantic Ocean. Then, westwards until the 28°W meridian, the difference, in the case of K_v = 10^{-3} m^2/s, drops to 4 μatm. The pCO_2 obtained with K_v = 5 x 10^{-4} m^2/s are smaller than those with K_v = 10^{-3} m^2/s east of 11°W; but west of 11°W, the reverse is true. Along the 4°W, 11°W, 23°W, and 28°W meridians, the fit between simulated and "observed" CO_2 fluxes is good (difference no larger than 0.7 mmol/m^2 day in both cases K_v = 5 and 10 x 10^{-4} m^2/s). Further west along the 35°W meridian, the model overestimates the observed CO_2 fluxes by as much as 1.25 mmol/m^2 day (case of a small K_v).

4.2. Sensitivity to the Meridional Flow Field

A few simulations have been performed where we decreased the nominal meridional water fluxes at the southern boundary of the 0°-2°S band by 10, 30, and 50% and consequently readjusted the northern fluxes in order to ensure mass conservation. Results in the 50% decrease case are shown in Figure 8 (case of K_v = 5 x 10^{-4} m^2/s). Alteration of these meridian fluxes does not induce any major change on the simulated time course of nitrate, total CO_2, water pCO_2, and CO_2 flux to the atmosphere.

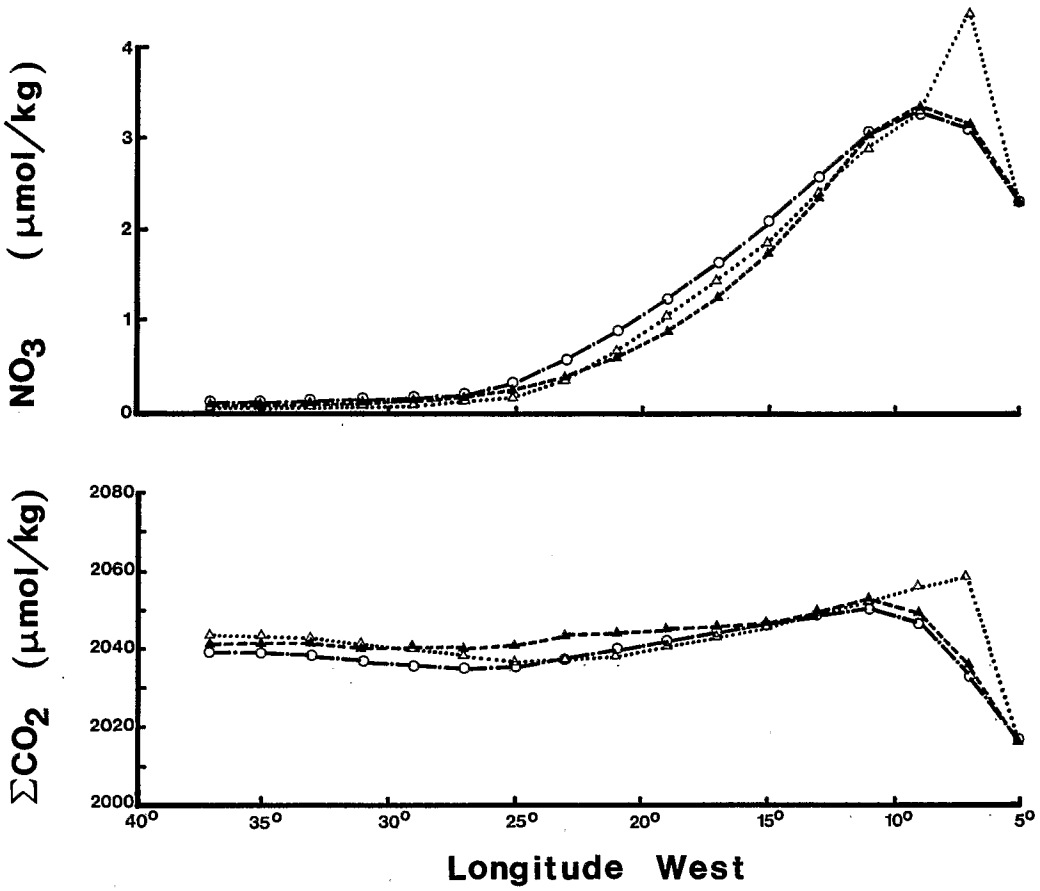

Fig. 8. NO_3^- (µmol/kg), ΣCO_2 (µmol/kg), pCO_2 (µatm), and CO_2 flux from the ocean to the atmosphere (mmol/m^2 day) versus longitude within the Equator-2°S band. Simulation results, in the case of $K_v = 5 \times 10^{-4}$ m^2/s, with the nominal meridional flow field (solid triangles), with a 50% decrease in the nominal meridional water fluxes at the southern boundary (2°S) (open circles), and with the flow field derived from a two-layer nonlinear (2LA) model (open triangles).

4.3. Sensitivity to the Zonal Flow Field

We investigate here whether the model is sensitive to the prescribed zonal flow field. We therefore use a different representation of the velocity field of the SEC derived from a two-layer nonlinear model (hereafter the 2LA model: P. Andrich, unpublished data, 1987). The basic physical assumptions of the model are those of Cane [1979]. The ocean is divided into two dynamically active layers. The surface layer (thickness H_1) is considered to be representative of the oceanic mixed layer and the second one (H_2), of the equatorial thermocline zone. The deep ocean is at rest with no pressure gradient. The wind stress is distributed in the surface layer as a body force. The wind stress is from the European Center for Medium Range Weather Forecasting (ECMRWF) and defined as the FOCAL-SEQUAL product 1: It does not include ship observations obtained during the FOCAL cruises. The thickness H_1 is taken constant in space and time at 30 m. Monthly mean velocities for the month of July 1983 are displayed in Figure 9. They are weaker than the ship drifts, since they constitute an average over the upper 30 m of the water column.

The box average zonal velocity is taken as the 2LA model component along the 1°S latitude circle each 2° of longitude. The meridional component of the velocity along the Equator is also from the 2LA model, and we deduce the component at 2°S to satisfy mass continuity in the 2° x 2° box. The time evolution of nitrate and total CO_2 concentrations, water pCO_2, and CO_2 flux at the air-sea interface is not affected by the change in zonal flow field west of 8°W (Figure 8, case of $K_v = 5 \times 10^{-4}$ m^2/s). On the contrary, east of 8°W, a high peak in all tracer concentrations is simulated, thereby inducing high water pCO_2 and CO_2 flux values. This difference is explained by the relative importance of the zonal change of the box volume (kept identical in both experiments) to the meridional transport (weaker in the last case).

5. Discussion

As a whole, the model simulates the observed data rather well. The results are fairly insensitive to most a priori choices. The study shows that among all processes parameterized in the model, divergence of advection, vertical mixing, and biological activity affect the model response most. In the runs we performed, we

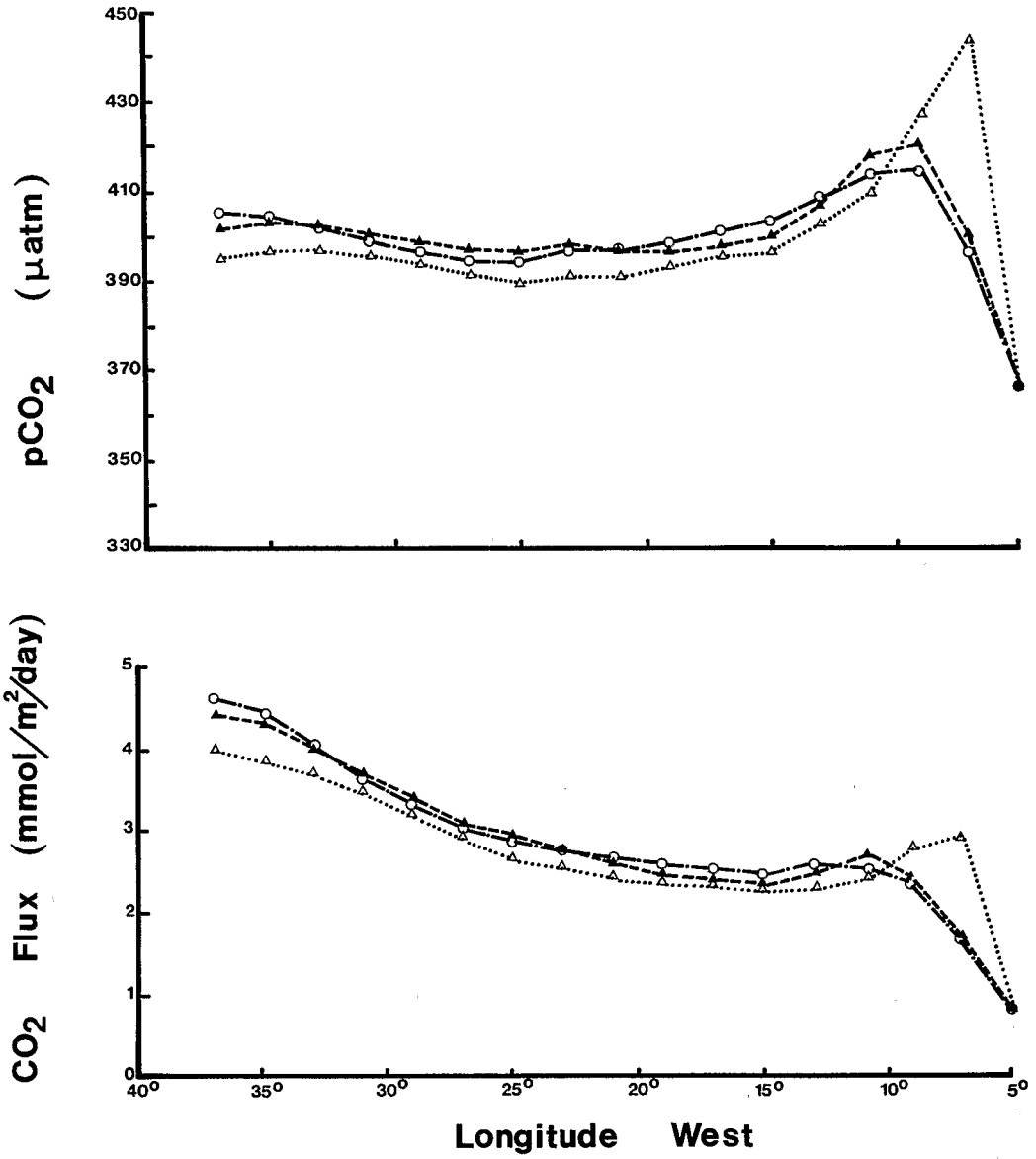

Fig. 8 (continued)

allowed the vertical eddy diffusion coefficient K_v values to vary between 10^{-4} and 10^{-3} m^2/s. Reasonable fits to the data were achieved with K_v values of 5 x 10^{-4} and 10^{-3} m^2/s (Figure 7). Measurements show that the vertical eddy diffusion coefficient varies considerably in the tropical ocean. It usually has large values in the mixed surface layer but very small values below the thermocline [Pacanowski and Philander, 1981]. Crawford and Osborn [1979a, b] suggested that in the Atlantic 13°C thermostad, K_v varies from 2 to 11 x 10^{-4} m^2/s. At the core of the EUC, the value is of order 10^{-4} m^2/s, and above the core it varies from 8 to 100 x 10^{-4} m^2/s. Katz et al. [1979] calculated a K_v value above the EUC equal to 1.5 x 10^{-4} m^2/s. Thus our choice lies on the lower side of this range of estimates.

From $J_{NO_3^-}$, one can calculate, at each 2° step, the new production J_C (in mol $C/m^2/yr$) as $J_{NO_3^-}$.C/N divided by the constant 2° x 2° box surface area. Figure 10a shows the variation of J_C versus longitude for the two runs K_v = 5 and 10 x 10^{-4} m^2/s. The striking feature is a dome in the eastern region between 4°W and 11°W followed by a decrease from the east to the west in both runs. In the case of large K_v and J_{max}, the decrease is rather steep from 36 mol $C/m^2/yr$ at 11°W to 10 mol $C/m^2/yr$ at 25°W, whereas J_C varies with a smoother slope from 18 to 7 mol $C/m^2/yr$ between 11°W and 25°W, in the case of small K_v and J_{max}. At the western end of the SEC, before it divides into the Brazil and North Brazil currents, new production values drop to 1-3 mol $C/m^2/yr$. We have seen that when a K_v value is assigned in a simulation, one J_{max} value provides the best fit to the data. For example, a J_{max} of 5 x 10^9 µmol N/s corresponds to a new production value J_C of ≈ 21 mol $C/m^2/yr$.

As explained before, the parameterization of biological activity was made using two different approaches: (1) a Michaelis-Menten function for nutrient uptake using the NO_3^- data in the

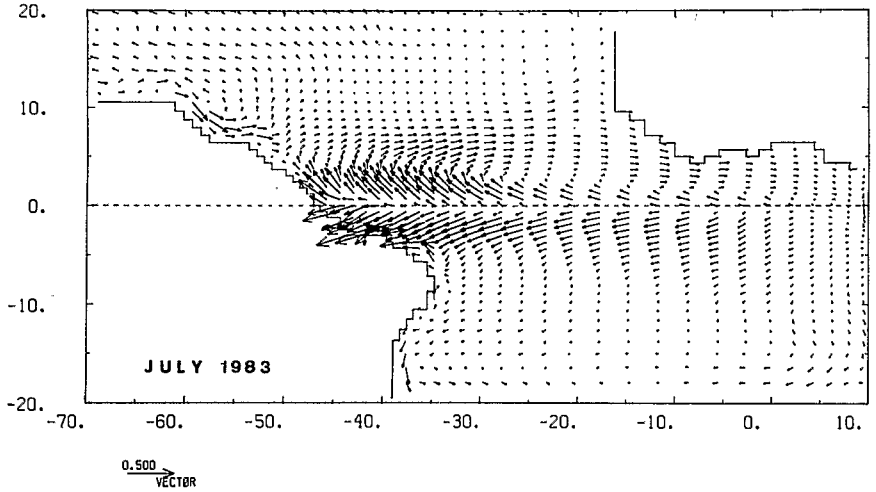

Fig. 9. Monthly mean velocities for the month of July 1983 derived from a two-layer nonlinear model (P. Andrich, unpublished data, 1987). They represent an average over the upper 30 m of the water column. Speed is proportional to the length of the tail of a vector.

Equator-2°S band, and (2) the same Michaelis-Menten function as case 1 but with NO_3^- as a state variable of the model (see section 2.4.1). We found from east to west in case (1) J_C values ranging from 17 to 6 mol C/m^2/yr with a dome (18 mol C/m^2/yr) at 11°W, and in case 2 from 17 to ≈ 1 mol C/m^2/yr with the same dome as in case 1. The difference between 6 and 1 mol C/m^2/yr in the western Atlantic Ocean is due to very low simulated NO_3^- values (0.05 μmol/kg) compared with the data (0.2 μmol/kg). Still, it is quite encouraging that the J_C estimates in case 2, the least constrained case, compare reasonably well with the other case.

Finally, the range of J_C values looks consistent with the range of estimates of total primary production in the tropical Atlantic Ocean [Corcoran and Mahnken, 1969; Voituriez and Herbland, 1981, Berger et al., 1987], using the relationship between new and total productions determined by Eppley and Peterson [1979]. Figure 10b is a map of total primary production during August 1963 [Voituriez and Herbland, 1981] showing a decrease in production from east to west. This map gives a minimum assessment of the equatorial production, since in the summer of 1963 there was no appearance of active upwelling, and higher values (≈ 100 mol C/m^2/yr) were measured in July 1977 [Voituriez and Herbland, 1977]. If one calculates the ratio of new (nitrate-based) (from Figure 10a, with J_{max} = 5 x 10^9 μmol/s, for instance) over total production (from Figure 10b), one finds a decreasing ratio from east to west (≈ 30% in the Gulf of Guinea, ≈ 20% at 23°W, and ≈ 10% at 35°W).

The capacity of the model to represent the observed data, as well as the correct orders of magnitude of the adjustable parameters K_v and J_{max} as compared with independent estimations, suggests that all the major terms which control the equatorial Atlantic CO_2 values are taken into account. The relative importance of the terms which drive the variations of ΣCO_2 and nitrate values is represented in Figure 11. For ΣCO_2 (Figure 11a), the advective transports are the dominant terms. This includes tracer input and withdrawal due to the zonal change of the box volume (the drop of these terms near 28°W is due to the vanishing meridional flux there). The sinks due to biological consumption approximately balance the inflow from the core of the EUC by diapycnal mixing. However, near 10°-20°W, consumption uses only about 30% of the total nitrate input to the box. The remaining part leaves the domain northward with the flow field. Degassing and isopycnal mixing play a minor role in the total CO_2 budget. In their analysis of CO_2 degassing in the tropical Atlantic, Smethie et al. [1985] argue that warming of the surface water during its westward transport is the dominant cause for the increase of CO_2 partial pressure. Andrié et al. [1986] argue that the gas exchange flux is further increased by the wind effect on the gas transfer coefficient. Both effects are included in our calculations.

What our model shows is that meridional divergence is an essential term in the CO_2 budget [Smethie et al. [1985] only partially take this effect into account via the salinity change], so that important seasonal and interannual variations could result from variations of the flow field. The doming of the 24.90°/$_{oo}$ isopycnal level near 10°-15°W, and the resulting surface pCO_2 increase are good examples of that effect. The kinematic box model developed herein is not really Lagrangian, as the box only follows the zonal displacement. In addition, we assumed that the flow field was constant during the time required for a parcel of surface water to flow zonally from 4°W to 38°W. This time is about 5 months with the climatological surface currents and almost 8 months with the 2LA model currents. The latter are, a priori, more suitable to advect the box, since they represent a vertical integral. These times are consistent with a travel time of about 6 months across the basin, as indicated by the drifting buoy trajectories for the deployment of late June 1983 [Reverdin and McPhaden, 1986]. During such a period, the flow field cannot be considered constant. Nevertheless, the conclusion

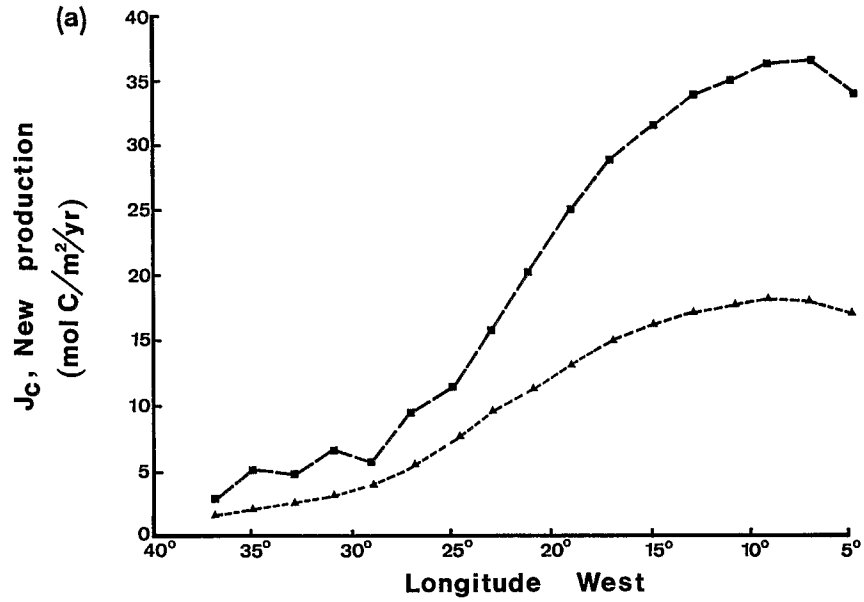

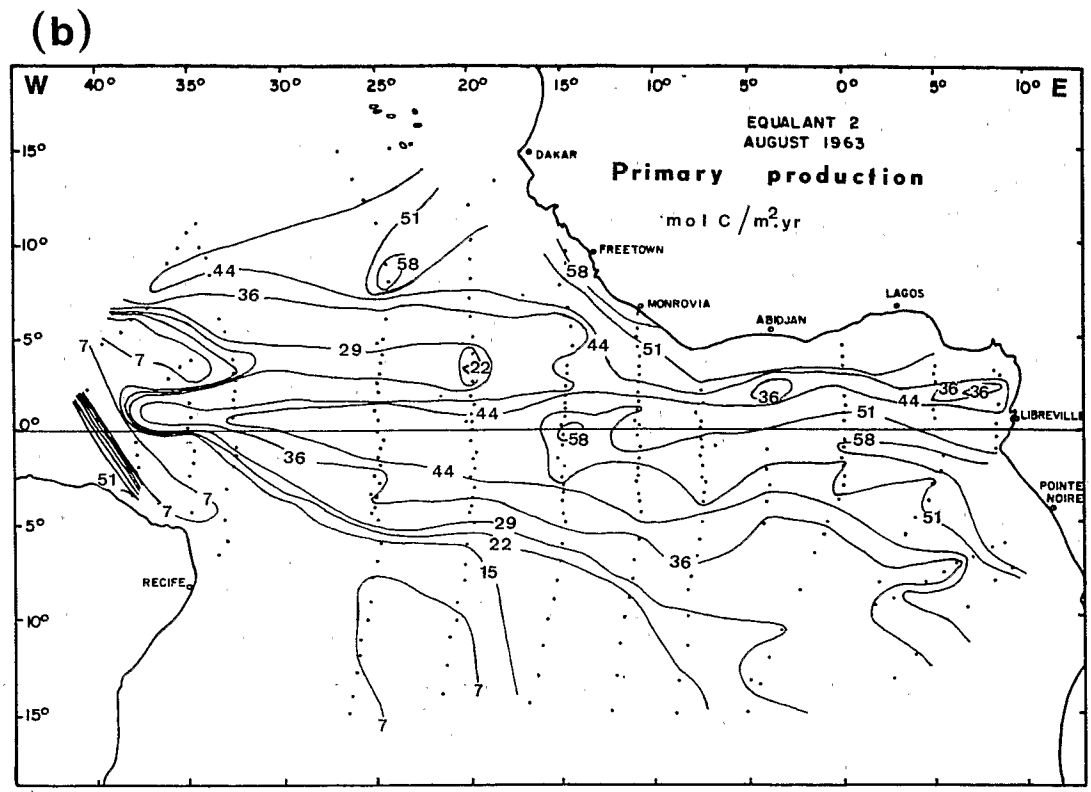

Fig. 10. (a) New production J_C (mol C/m^2 yr) as calculated by the model versus longitude for two cases: $K_v = 5 \times 10^{-4}$ m^2/s (triangles) and $K_v = 10 \times 10^{-4}$ m^2/s (squares) within the Equator-2°S band (NO_3^- as a state variable of the model, see section 2.4.1). (b) Map of total primary production (mol C/m^2 yr) during Equalant 2 (August 1963) [from Voituriez and Herbland, 1981].

concerning the influence of the different parameters remains valid.

Finally, current profiler measurements during FOCAL 4 show a surface eastward component along the 11°W meridian between 0°30S and 2°S, whereas within the 0°-2°S band at 4°W, only the westward SEC is present [Hénin et al., 1986]. This can be due to shoaling of the core of the eastward EUC at 11°W of longitude. Indeed high salinities, significant cooling, and nitrate enrichment due to the equatorial upwelling are well marked at 10°-11°W [Hénin et al., 1986, Figure 2]. They are also apparent at 4°W but a little further south (1°S-2°S). The position of the sea surface

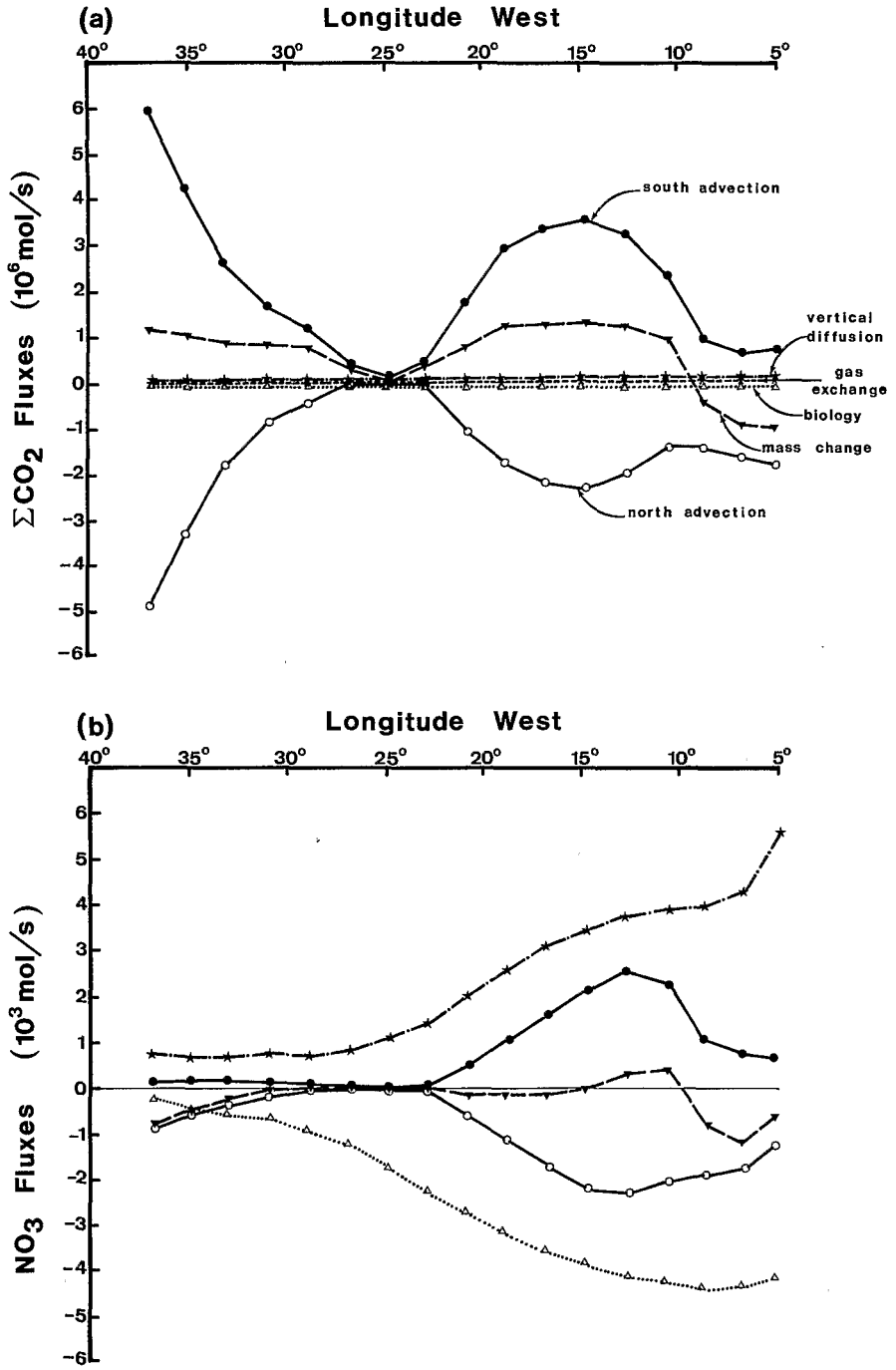

Fig. 11. Longitudinal variations of the various fluxes controling the balance of (a) total CO_2 (10^6 mol/s) and (b) nitrate (10^3 mol/s), in the case of $K_v = 5 \times 10^{-4}$ m^2/s within the Equator-2°S band. Flow field derived from Richardson and Walsh [1986].

temperature front in July 1983 corroborates this explanation [Legeckis and Reverdin, 1986].

This study shows that, once K_v is fixed by the parameterization of the dynamical model, only one parameter, J_{max}, has to be adjusted to satisfy the surface nitrate and CO_2 system. A similar work, to be performed with the other FOCAL data [FOCAL 2, January-February 1983, FOCAL 6, January-February 1984, and FOCAL 8, July-August 1984] should allow a test of this result and help evaluate whether a seasonal variation of J_{max} is measurable for the equatorial band. In addition, it is not obvious whether the same production function should be used out of this equatorial band.

Acknowledgments. We thank Claude Oudot (ORSTOM) for providing the FOCAL data, and Christine Provost for critical reading of the manuscript. This work was supported by a grant

from the Centre National de la Recherche Scientifique to UM 39.

References

Andrié, C., C. Oudot, C. Genthon, and L. Merlivat, CO_2 fluxes in the tropical Atlantic Ocean during FOCAL cruises, J. Geophys. Res., 91, 11,741-11,755, 1986.

Arnault, S., Variation saisonnière de la topographie dynamique et de la circulation superficielle de l'océan Atlantique tropical, thèse de 3ème cycle, 198 pp., Univ. Pierre et Marie Curie et Mus. d'Hist. Natur. Paris, 1984.

Berger, W. H., K. Fisher, C. Lai, and G. Wu, Ocean productivity and organic carbon flux, I, Overview and maps of primary production and export production, SIO Ref. Ser. 87-30, 67 pp., Scripps Inst. of Oceanog., Univ. of Calif., San Diego, 1987.

Broecker, W. S., and T. -H. Peng, Gas exchange rates between air and sea, Tellus, 26, 21-35, 1974.

Broecker, W. S., and T. -H. Peng, Tracers in the Sea, 690 pp., Lamont-Doherty Geological Observatory, Palisades, N. Y., 1982.

Broecker, W. S., and T. Takahashi, The relationship between lysocline depth and in situ carbonate ion concentration, Deep Sea Res., 25, 65-95, 1978.

Cane, M. A., The response of an equatorial ocean to simple wind stress patterns, I, Model formulation and analytic results, J. Mar. Res., 37, 233-252, 1979.

Corcoran, E. F., and C. V. W. Mahnken, Productivity of the tropical Atlantic Ocean, Proceedings of the Symposium on the Oceanography and Fisheries Resources of the Tropical Atlantic, pp. 57-67, UNESCO, 1969.

Crawford, W. R., and T. R. Osborn, Microstructure measurements in the Atlantic Equatorial Undercurrent during GATE, Deep Sea Res., 26, Suppl. 2, 285-308, 1979a.

Crawford, W. R., and T. R. Osborn, Energetics of the Atlantic equatorial currents, Deep Sea Res., 26, Suppl. 2, 309-324, 1979b.

Culkin, F., The major constituents of seawater, in Chemical Oceanography, chap. IV, 1st ed., edited by J. P. Riley and G. Skirrow, pp. 121-161, Academic, San Diego, Calif., 1965.

Dugdale, R. C., and J. J. Goering, Uptake of new and regenerated forms of nitrogen in primary productivity, Limnol. Oceanogr., 12, 196-206, 1967.

Eppley, R. W., and B. J. Peterson, Particulate organic matter flux and planktonic new production in the deep ocean, Nature, 282, 677-680, 1979.

Eppley, R. W., J. N. Rogers, and J. J. McCarthy, Half saturation constants for uptake of nitrate and ammonium by marine phytoplankton, Limmol. Oceanogr., 14, 912-920, 1969.

Gargett, A. E., Vertical eddy diffusivity in the ocean interior, J. Mar. Res., 42, 359-393, 1984.

Hénin, C., P. Hisard, and B. Piton, Programme Français Océan-Climat Atlantique Equatorial FOCAL, vol. 1, Observations hydrologiques dans l'Océan Atlantique équatorial (juillet 1982-août 1984), Trav. Doc., 196, 194 pp, ORSTOM, Paris, 1986.

Hisard, C., and C. Hénin, Zonal pressure gradient, velocity and transport in the Atlantic equatorial undercurrent from FOCAL cruises (July 1982-February 1984), Geophys. Res. Lett., 11, 761-764, 1984.

Katz, E. L., J. G. Bruce, and B. D. Petrie, Salt and mass flux in the Atlantic equatorial undercurrent, Deep Sea Res., 26, Suppl. 2, 137-160, 1979.

Keeling, C. D., and B. Bolin, The simultaneous use of chemical tracers in oceanic studies, 1, General theory of reservoir models, Tellus, 19, 566-581, 1967.

Legeckis, R., and G. Reverdin, Long waves in the equatorial Atlantic Ocean during 1983, J. Geophys. Res., 92, 2835-2842, 1987.

Liss, P. S., Processes of gas exchange across an air-water interface, Deep Sea Res., 20, 221-238, 1973.

Liss, P. S., and L. Merlivat, Air-sea gas exchange rates: Introduction and synthesis, in The Role of Air-Sea Exchange in Geochemical Cycling, Adv. Sci. Inst. Ser., edited by P. Buat-Ménard, pp. 113-127, D. Reidel, Hingham, Mass., 1986.

Lyman, J., Buffer mechanism of seawater, Ph.D. thesis, 196 pp., Univ. of Calif., Los Angeles, 1956.

Mehrbach, C., C. H. Culberson, J. E. Hawley, and R. M. Pytkowicz, Measurement of the apparent dissociation constants of carbonic acid in seawater at atmospheric pressure, Limnol. Oceanogr., 18(6), 897-907, 1973.

Oudot, C., R. Gerard, A. Herbland, A. Le Bouteiller, Y. Montel, P. Morin, and P. Raimbault, Programme Français Océan-Climat Atlantique Equatorial FOCAL, vol. 2, Distributions verticales des propriétés physico-chimiques et de la biomasse végétale dans l'océan Atlantique tropical (Programme PIRAL), Trav. Doc., 209, 215 pp, ORSTOM, Paris, 1988.

Pacanowski, R. C., and S. G. H. Philander, Parameterization of vertical mixing in the numerical models of tropical oceans, J. Phys. Oceanogr., 11, 1443-1451, 1981.

Provost, C., and M. -S. Suk, About a diagnostic analysis of the historical hydrographic data in the tropical Atlantic, Ann. Geophys., 58(3), 221-238, 1987.

Reverdin, G., and M. J. McPhaden, Near-surface current and temperature variability observed in the equatorial Atlantic from drifting buoys, J. Geophys. Res., 91, 6569-6581, 1986.

Richardson, P. L., and T. K. McKee, Average seasonal variation of the Atlantic equatorial currents from historical ship drifts, J. Phys. Oceanogr., 14, 1226-1238, 1984.

Richardson, P. L., and D. Walsh, Mapping climatological seasonal variations of surface currents in the tropical Atlantic using ship drifts, J. Geophys. Res., 91, 10,537-10,550, 1986.

Smethie, W. M. Jr., T. Takahashi, D. W. Chipman, and J. R. Ledwell, Gas exchange and CO_2 flux in the tropical Atlantic Ocean determined from ^{222}Rn and pCO_2 measurements, J. Geophys. Res., 90, 7005-7022, 1985.

Takahashi, T., W. S. Broecker, and S. Langer, Redfield ratios based on chemical data from isopycnal surfaces, J. Geophys. Res., 90, 6907-6924, 1985.

Tourre, Y., and P. Chavy, Programme Français Océan-Climat Atlantique Equatorial FOCAL, Mean surface winds during the FOCAL campaigns, Kinematic analyses, Rapport interne, 20 pp., ORSTOM, Paris, 1986.

Voituriez, B., Les variations saisonnières des courants équatoriaux à 4°W et l'upwelling équatorial du Golfe de Guinée, II, Le courant équatorial Sud, Oceanogr. Trop., 18, 185-199, 1983.

Voituriez, B., and A. Herbland, Etude de la production pélagique de la zone équatoriale de l'Atlantique à 4°W, I, Relations entre la structure hydrologique et la production primaire. Cah. ORSTOM, Ser. Oceanog., 15, 313-330, 1977.

Voituriez, B., and A. Herbland, Primary production in the tropical Atlantic Ocean mapped from oxygen values of Equalant 1 and 2 (1963), Bull. Mar. Sci., 31(4), 853-863, 1981.

Voituriez, B., A. Herbland, and R. Le Borgne, L'upwelling équatorial de l'Atlantique Est pendant l'expérience Météorologique Mondiale (PEMG), Oceanol. Acta, 5, 301-314, 1982.

Weiss, R. F., Carbon dioxide in water and seawater: The solubility of non-ideal gas, Mar. Chem., 2, 203-215, 1974.

P. Andrich, Laboratoire d'Océanographie Dynamique et de Climatologie, Université Pierre et Marie Curie, 4 place Jussieu, 75252 Paris Cedex 05, France.

C. Andrié, Laboratoire de Géochimie Isotopique-LODYC: Laboratoire d'Océanographie Dynamique et de Climatologie, Département de Physico-Chimie, CEN Saclay, 91191 Gif-sur-Yvette, France.

V. C. Garçon, L. Martinon, and J.-F. Minster, UM 39, Centre National d'Etudes Spatiales/GRGS: Groupe de Recherche de Géodésie Spatiale, 18 avenue Edouard Belin, 31055 Toulouse Cedex, France.

(Received February 4, 1988;
accepted March 21, 1988.)